Chapter 2

Nanocrystallization of Metallic Glasses Followed by *in situ* Nuclear Forward Scattering of Synchrotron Radiation

Marcel B. Miglierini and Vít Procházka

Additional information is available at the end of the chapter

http://dx.doi.org/10.5772/66869

Abstract

A central problem in nanotechnology is the understanding of structure-to-properties relationship. This is essential for tailoring the functionalities, efficiency, and performance of the near-future materials. Here, hyperfine interactions can be employed as they instantly reflect the state of structural arrangement. Examination of the corresponding hyperfine parameters during nanocrystallization through the use of the so-called nuclear forward scattering (NFS) of synchrotron radiation is now possible. One can follow separately structural evolution of different sites of the ^{57}Fe probe atoms. Structural transformations in metallic glasses including nanocrystallization were investigated by NFS to fine details that are completely hidden when conventional analytical tools are employed. Systematic analyses of NFS time-domain patterns provided an opportunity to study independently the role of structurally different regions. The latter comprise amorphous residual matrix, newly formed nanocrystallites, and interface regions. Different amounts of iron atoms located at the nanograins' surfaces and in their core were observed for different crystallization conditions, viz. temperature, time, and/or magnetic field. The application of in situ NFS experiments has a huge potential for observations of the evolution of phase transformations in real time performed on fly during short time intervals.

Keywords: metallic glasses, nanocrystallization, structural transformation, nuclear forward scattering, synchrotron radiation

1. Introduction

Understanding the structure-to-properties relationship is one of the most important problems in materials research. Thorough knowledge on structural arrangement namely in disordered systems like amorphous metallic alloys is essential for tailoring the functionalities, efficiency

and performance of devices based on these materials. Because of their amorphous nature, these metallic alloys are often referred to as metallic glasses (MGs). Their suitable chemical composition ensures formation of crystallites that grow inside the amorphous matrix during thermal annealing and measure only several nanometres in size. Due to these dimensions, they provide beneficial magnetic properties in these the so-called nanocrystalline alloys (NCAs). At the same time, formation of nanograins stabilizes the whole structure against further thermal deterioration.

Changes in microstructure, crystallization behaviour, and magnetic states of NCAs have suggested that interface regions between nanocrystalline grains and the surrounding amorphous matrix play a significant role in propagation of ferromagnetic exchange interactions between the nanograins through the residual amorphous matrix. In order to understand the process of nanocrystallization, it is inevitable to study it in situ, that is, *during* annealing. For this purpose, we use in situ nuclear forward scattering (NFS) of synchrotron radiation. NFS provides information on changes in structural arrangement via hyperfine interactions in real time. In this respect, it is superior to other in situ techniques.

This contribution aims at providing insight into the studies of structural transformations that are taking place in iron-based metallic glasses exposed to elevated temperatures. Evolution of nanocrystalline grains during dynamical increase of temperature and isothermal annealing is discussed by the help of NFS technique. Before doing that, we provide brief description of MGs and NCAs. In addition, a short review of the methods used for their structural characterization is also offered. Prior to introducing the results of NFS investigations, basic principles of this method are presented, too.

2. Metallic glasses and nanocrystalline alloys

Fe-based ferromagnetic MGs possess interesting physical properties that are superior to those of their crystalline counterparts. This is mainly due to lack of any long-range order, that is, periodic atomic arrangement that is particularly important for their magnetic performance [1, 2]. They are often employed as magnetic shielding, transformer cores, sensors, recording media [3] as well as in other technical applications [4].

Structural changes that can occur in MGs when they are exposed to high enough temperatures for extended operational times degrade their working parameters. This becomes particularly important with the onset of crystallization. On the other hand, suitable chemical compositions of some MGs assure formation of crystalline grains with typical sizes of up to several tens of nanometres. The resulting NCAs represent a novel type of materials whose physical properties can be tailored not only by appropriate chemical elements but also by varying the size of the nanocrystalline grains, their morphology, and the composition of nanograins. NCAs all can be prepared from MGs by annealing under well-defined conditions (temperature and time) which ensure controlled temperature treatment and trigger partial crystallization. In opposite to MGs, the magnetic parameters of NCAs do not substantially deteriorate at elevated temperatures [5]. Therefore, a comprehensive understanding of the

evolution of nanograins during nanocrystallization is essential in order to understand, optimize, and conserve the unique magnetic properties exhibited by metallic glasses and/or their nanocrystalline counterparts.

Though studied already for decades, MGs still attract the interest of researchers due to their unique physical properties [6]. A central problem seems to be the understanding of structure-to-properties relationship namely when MGs are transformed into NCAs. This is essential for tailoring the functionalities, efficiency, and performance of these near-future materials. These phenomena are routinely studied in a steady state, that is, once the particular structural arrangement is achieved, it is correlated with the resulting physical properties. Less attention is paid to the investigation of transient states that temporarily exist *for the period of* a structural transformation. Such an approach is, however, a demanding experimental task.

Broad arsenal of diagnostic techniques is applied in order to understand the process of transformation from MG into NCA structural arrangement, that is, the crystallization of MGs [7–9]. Yet, majority of these techniques provide only *ex situ* information as the time needed for acquisition of sufficiently good statistics of the experimental data frequently extends over several tens of minutes or even hours. In addition, some of the imaging techniques require special treatment for sample preparation which can substantially affect their structure. Subsequently, in situ investigation of the induced structural transformations using these techniques is not possible in real time, and the study of dynamics and/or kinetics of crystallization process is not so straightforward.

Methods like DSC or magnetic measurements can examine materials in real time and, thus, provide in situ investigations. However, they scan the whole bulk of the investigated systems. As a result, the obtained information is averaged over all structurally different regions which are present in the studied system. That is why in situ characterization of structural transformations during crystallization of MGs is an experimental challenge.

Along with conventional analytical tools, also sophisticated and advanced techniques like atom probe tomography are employed [10]. The use of in situ characterization techniques is, however, still limited to diffraction of synchrotron radiation [11–13]. Recently, more sophisticated techniques of real-time in situ synchrotron X-ray tomographic microscopy [14] and combination of time-resolved X-ray photon correlation spectroscopy and high-energy XRD [15] were applied. All these studies which make use of very up-to-date synchrotron-based approaches provide valuable information of amorphous structures by revealing complex atomic rearrangements even though no well-defined structural positions exist in MGs.

Though X-ray diffraction based techniques are capable of in situ investigations, they do not provide site-specific information as the signal is averaged over the distribution of electron densities. From this point of view, use of local probe techniques such as Mössbauer spectroscopy offers unique opportunities to access both magnetic properties and structural states of the investigated material [16]. The relatively long acquisition times of a conventional Mössbauer spectrum (up to several hours), however, limit the application of this technique only to samples in steady equilibrium conditions. This substantially disables monitoring of the crystallization process itself.

3. Nuclear forward scattering of synchrotron radiation

Progress in synchrotron sources of radiation has introduced the method of nuclear forward scattering of synchrotron radiation [17]. This method uses ^{57}Fe resonant nuclei as probes of the local magnetic and electronic properties in the investigated samples. Thus, information on hyperfine interactions similar to Mössbauer spectrometry is readily available. Application of NFS is helpful in revealing the mutual relation between the magnetic arrangement and the structure of the studied materials. Due to extremely high brilliance of the latest synchrotron sources, studies can be performed in dynamic in situ regimes. Rapid recording of experimental data allows for direct observation of dynamical processes that are taking place *during* heat treatment [18–22].

In this contribution, we discuss time aspect of NFS which enables time-dependent processes to be followed in real time. We demonstrate them using dynamical and kinetics processes that are taking place during nanocrystallization of selected MGs. Before doing so, let us mention another important technique which exploits nuclear properties of ^{57}Fe resonant nuclei that are activated by synchrotron radiation. It is the so-called nuclear inelastic scattering (NIS) of synchrotron radiation. It enables studies of the dynamics of NCAs via atomic vibrations and densities of phonon states [23, 24]. Because the time needed for acquisition of experimental data is still rather long, time-dependent NIS investigations are only evolving.

NFS belongs to the family of nuclear resonant scattering processes [25]. This technique can be considered as a full analogue of Mössbauer spectrometry [26]. It is especially useful under extreme conditions including high temperature, pressure, and/or magnetic fields when the space with such an environment is very limited, and hence, the sample can be as small as several tens of micrometers. High brilliance of synchrotron sources enables sufficient data counts even from such spatially limited regions. NFS permits on fly inspection of structural and/or magnetic arrangement that continuously evolves with changing temperature/time. In this respect, it is superior to other in situ techniques.

Energetic levels of atomic nuclei are exposed to the so-called hyperfine interactions. The latter are due to an effective field that originates from the presence of surrounding atoms, their electronic shells, and/or external fields. Consequently, nuclear levels are shifted and/or split, and in this way, they sensitively reflect chemical and topological states of the resonant atoms. Effect of the three main types of hyperfine interactions, viz. electric monopole, electric quadrupole, and magnetic dipole interaction upon nuclear levels, is schematically drawn in the upper part of **Figure 1**. Possible transitions among nuclear levels are indicated by arrows.

Electric monopole interaction is proportional to charge density at the nucleus and provides information about valence and spin states of the resonant atom, about its electronegativity and chemical bonding. Electric quadrupole interaction is governed by electric field gradient acting upon the nucleus and reflects the charge distribution. It is related to oxidation state, spin state as well as symmetry of the positions of resonant atoms. Magnetic dipole interaction

http://dx.doi.org/10.5772/66869

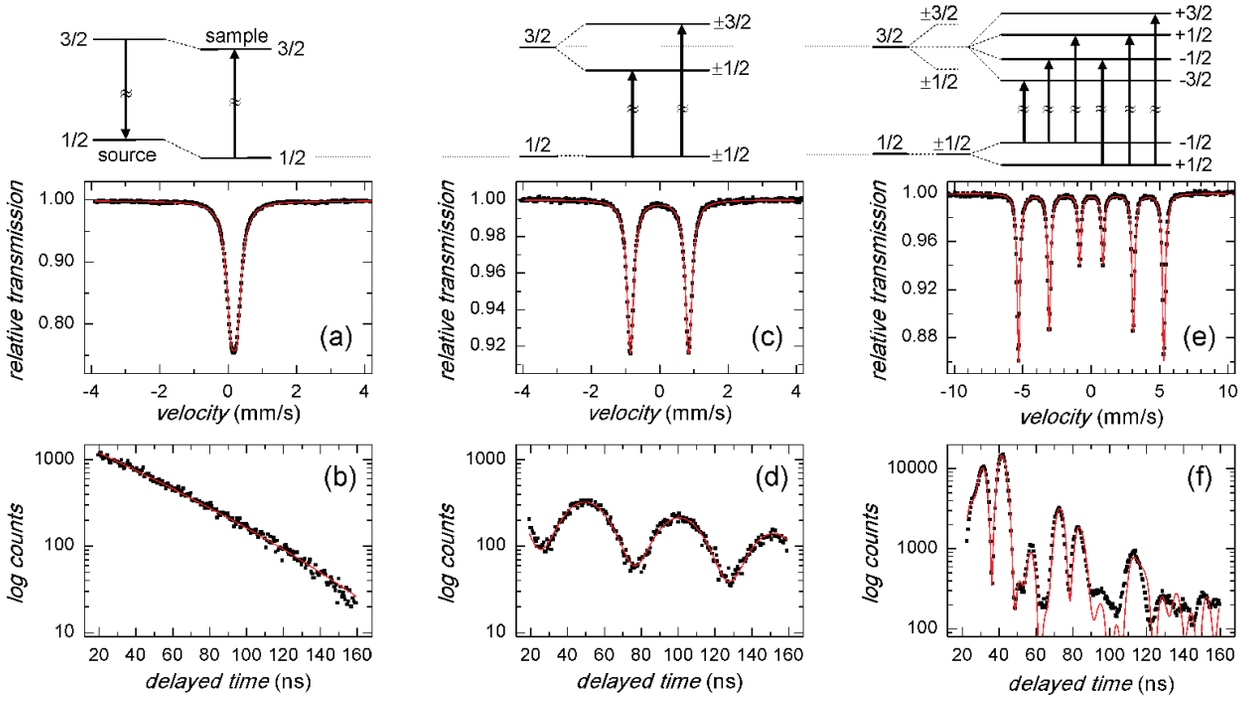

Figure 1. Typical representatives of the basic shapes of Mössbauer spectra recorded in energy domain (middle row) and the corresponding NFS time-domain patterns (bottom row). They demonstrate presence of electric monopole (a and b), electric quadrupole (c and d), and magnetic dipole (e and f) hyperfine interactions that cause the shift/splitting of nuclear levels as drawn in the top row.

originates from coupling between nuclear magnetic moment and effective magnetic field at the nucleus due to spin polarization. Thus, information on magnetic states of the resonant atoms, which is, moreover, temperature-dependent, is readily available. It is noteworthy that resonant atoms located in defined structural positions (e.g., in a crystalline lattice) feature individual set of hyperfine interactions and, hence, corresponding spectral parameters. The latter are like fingerprints which uniquely identify these particular atomic sites and can be derived either from Mössbauer spectra or from NFS experiments. In addition, relative fractions of such structurally different positions in the investigated samples are related to the contribution of the particular spectral components.

Transitions between ground and excited states of the resonant nuclei are accompanied by absorption and emission of photons with precise energy that is typically several tens of keV. In conventional Mössbauer spectrometry, resonance absorption of the emitted gamma photons by a particular absorber (i.e., the investigated sample) is achieved by fine tuning of their energy through a Doppler effect [27]. As a source of radiation, suitable radioactive nuclides are used. Splitting of nuclear energy levels is of the order of several hundreds of neV and is reflected via corresponding hyperfine parameters in the associated Mössbauer spectra that are recorded in energy domain. The resulting basic shapes of Mössbauer spectra are depicted in the middle row of **Figure 1**.

If only electric monopole hyperfine interaction occurs, the corresponding Mössbauer spectrum shows only one line, the so-called singlet as seen in **Figure 1a**. Presence of electric quad-

rupole interaction at the resonating nuclei splits the excited level into two degenerating ones. Consequently, in the case of ^{57}Fe nuclei (nuclear spin 3/2 in the excited state and 1/2 in the ground state), two transitions are possible. Hence, a doublet of absorption Mössbauer lines is formed as seen in **Figure 1c**. Zeeman-split sextet is observed in **Figure 1e** when magnetic dipole interactions act upon the ^{57}Fe resonant nuclei. Presence of sextets in Mössbauer spectra indicates that the corresponding fraction of iron atoms (represented by a spectral area under the absorption lines) is ferro-, ferri-, or antiferromagnetically ordered. In real samples, any combination of the three basic spectral shapes is possible.

With the development of monochromators, synchrotron radiation turned out to be suitable candidate for replacing conventional radionuclide sources of photons. As schematically depicted in the upper part of **Figure 2**, bunches of accelerated particles (electrons) produce flashes of synchrotron radiation when they pass through undulators. Pulses of photons have typical duration of ~50 ps and repetition rate ~200 ns. Their energy is tuned to the requested Mössbauer transition using high-resolution monochromator that provides energies of photons within a bandwidth (ΔE_γ) of several meV. The pulse contains wider range of energies than is needed for excitation of available nuclear levels in the studied sample. It is drawn in the bottom part of **Figure 2** as a broad (blue) arrow and ensures immediate excitation of all nuclear transitions. Energy separation of nuclear levels due to hyperfine interactions is of the order of several hundreds of neV. Thus, not only the different transitions of the same nucleus but also all transitions of different nuclei are excited simultaneously at the *same time* upon an impingement of the synchrotron radiation pulse upon the sample. Let us remind that in Mössbauer spectrometry, nuclear transitions are excited sequentially one by one as the energy of photons varies over specific values.

In the time slot between two subsequent pulses, all excited nuclei emit the excess energy in a form of resonance delayed photons that are registered with a fast detector. The decay of the

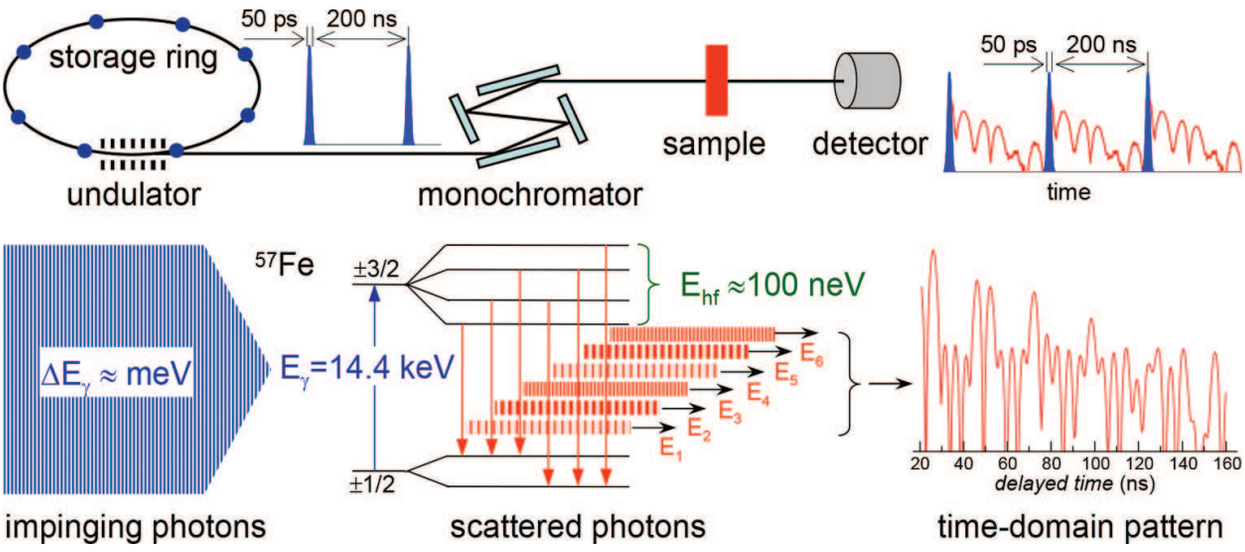

Figure 2. Basic layout of a typical NFS beamline with the major components (upper part). In the bottom part, magnetically split nuclear levels are simultaneously excited by a single pulse of incident synchrotron radiation with an energy spread $\Delta E_\gamma \approx$meV. Subsequent de-excitation provides scattered photons of different energies (E_1–E_6) that sum up to the NFS time domain pattern.

nuclear excited states reflects hyperfine interactions of the resonant nuclei. All de-excitation photons sum up and give rise to interference patterns in time domain as shown in the bottom row of **Figure 1**. In the following, we will call them *NFS time-domain patterns*.[1] The prompt excitation pulse sets the time zero. Due to its extremely high intensity the detector starts to count when only delayed photons are present which usually takes about 10–20 ns after the excitation.

The counts of delayed photons are registered as a function of time that has elapsed after the excitation. That is why NFS is sometimes referred to as Mössbauer spectrometry in time domain. Single transition is characterized by an exponentially decaying signal (linear in semi logarithmic scale, see **Figure 1b**). Multiple photons originating from multiple transitions exhibit characteristic beating of intensities called quantum beats. Their character is unique for particular hyperfine structure as demonstrated in **Figure 1d** and **f** for electric quadrupole and magnetic dipole interactions, respectively.

In general, any NFS time-domain pattern can be represented by some of the basic patterns plotted in the bottom row of **Figure 1** and/or a combination of them. In any case, they carry information on hyperfine interactions that are unique for individual atomic sites of the resonant atoms. Evaluation of experimental NFS data is performed by their fit to a suitably chosen theoretically calculated model. Each model consists of several sets of hyperfine parameters that are each ascribed to one particular atomic site. The obtained resulting parameters identify valence states, symmetry of charge distribution, and magnetic ordering. Phase composition of the material under study can be identified, and relative amount of each phase can be determined. Due to high site selectivity, we can study local electronic arrangement, and its fine distortions can be revealed. Some parameters like, for example, electric field gradient can be compared with the results of ab initio calculations. We can also easily follow magnetization of individual magnetic structures via hyperfine magnetic fields within magnetically active materials. So far, NFS technique was successfully applied to the study of different problems of materials research [28].

In this contribution, we present in situ NFS experiments that provide important information on the early stages of crystallization in MGs. This process can be monitored starting from formation of nucleation centres, their growth, and continuation towards equilibrium nanocrystalline state. Using this approach, the obtained results are not affected by a cooling process which is the case when ex situ experiments are employed.

4. Experimental particulars

4.1. NFS experiments

NFS experiments were performed at The European Synchrotron (ESRF), Grenoble using the Nuclear Resonance ID22N and ID18 stations. Excitation of the ^{57}Fe nuclear levels was accom-

[1]In a literature, one can find the expression 'NFS time spectrum'. However, the term 'spectrum' implies a dependence of counts upon energy. Because of the interference nature of NFS data, we find it physically inconsistent.

plished by a photon beam with the energy of 14.413 keV, flux of ~10^9 photons/s, and bandwidth of ~3 meV. The spot size of the synchrotron beam was of 0.7×0.3 mm^2. The estimated heat load at the sample was ~2 μW. Samples of the investigated MGs were placed in a vacuum furnace. Metallic glasses of $Fe_{90}Zr_7B_3$, $Fe_{81}Mo_8Cu_1B_{10}$, and $(Fe_{2.85}Co_1)_{77}Mo_8Cu_1B_{14}$ were prepared by the method of rapid quenching on a rotating wheel. The chosen compositions of MGs ensure formation of nanocrystalline alloys in which crystalline grains with the size of several nanometres are formed in the early stage of structural transformation. The obtained ribbons of MGs were ~1–2 mm wide and ~20 μm thick.

The maximum annealing temperature (up to ~700 °C) was limited by Kapton windows of the furnace. Nevertheless, this temperature was far behind the first crystallization step of the investigated MGs.

Two types of studies were performed: (i) dynamical time-dependent temperature increase/decrease and (ii) isothermal heat treatment. During the first type of experiments, temperature at the sample was continuously increasing with a ramp of 10 K/min. In the second type of experiments, the set temperature was reached with a ramp of 40 K/min and then maintained for up to 3 h. In both cases, NFS time-domain patterns were continuously recorded every minute during the whole duration of the experiment performed in transmission geometry. Thus, information on the bulk of the samples was obtained.

For the sake of more clear presentation of a high quantity of experimentally acquired time-domain patterns within a single experiment, we use contour plots to display the obtained NFS patterns. The latter are stacked with respect to the duration time of the experiment which constitutes the vertical axes of the contour plots. For dynamical experiments, this axis' scale is eventually converted into temperature values assuming a constant ramp of 10 K/min. The elapsed time is then given on the horizontal axes, and the counts of the registered photons (intensities) are colour coded in a logarithmic scale.

4.2. Physical models for the evaluation of NFS time-domain patterns

Fitting of the experimental data was performed by the CONUSS software package [29, 30] which is suitable for the evaluation of individual NFS time-domain patterns. However, the accomplished NFS experiments have provided a huge number of records. Typically, several tens (up to ~140) of time-domain patterns were obtained during one experiment. In order to process and subsequently evaluate such enormous data quantities, we have developed special software called Hubert [31]. The data evaluation is based on the conventional fitting route using CONUSS software. Hubert is designed for NFS time-domain patterns processing, time calibration, transformation from synchrotron output file format to experimental data file readable by CONUSS, a single time-domain pattern evaluation, large data sets analysis, and generation of hyperfine parameters distributions [32].

The investigated MGs are amorphous in the as-quenched state. Depending upon their composition, they are ferromagnetic ($(Fe_{2.85}Co_1)_{77}Mo_8Cu_1B_{14}$) and paramagnetic ($Fe_{90}Zr_7B_3$, $Fe_{81}Mo_8Cu_1B_{10}$) at room temperature. Consequently, the originally amorphous matrix is reproduced in the NFS time-domain patterns by distributions of hyperfine magnetic fields

and distributions of quadrupole splitting, respectively. With increasing temperature of measurement, magnetic dipole interactions eventually vanish, and only electric quadrupole ones are present. While the latter are fitted by distribution of quadrupole splitting, only this component is used to characterize the amorphous matrix in the particular MG.

After the onset of crystallization, that is, when the temperature of measurement reaches the first crystallization step, nanocrystalline grains emerge within the residual amorphous matrix. Because of the samples' composition, they are bcc-Fe or bcc-(Fe,Co) nanocrystals. Both exhibit rather strong magnetic dipole interactions which are represented by quantum beats with relatively high frequency of oscillations (see also **Figure 1f**). The associated fitting component features well-defined hyperfine magnetic field values, and it is ascribed to the inner part of the nanocrystalline grains with well-established crystalline symmetry. Atoms located at the surfaces of the nanograins exhibit broken symmetry, and they are referred to as interface regions [18]. Though still magnetic, their associated fitting component is represented by distributions of hyperfine magnetic fields with average field values lower by ~2–3 T than those of the core of the nanograins. Presence of this component was confirmed by conventional Mössbauer spectrometry [33].

To recapitulate the fitting models applied for the evaluation of the obtained NFS time-domain patterns, it should be noted that we distinguish three structurally different regions in the investigated samples. The first one is amorphous matrix which corresponds to the whole MG in its original as-quenched state as well as during moderate heat treatment up to the onset of crystallization. When the temperature exceeds the crystallization point, this structural component represents the residual amorphous matrix in the newly formed NCA. Both amorphous regions will be denoted in the following as AM—amorphous. Because AM can be either magnetic or paramagnetic (depending upon the sample's composition and/or temperature), this component is refined by distributions of hyperfine magnetic fields and quadrupole splitting, respectively.

Well-defined structural arrangement of the evolving nanocrystalline grains stands for the second structural region which will be labelled as CR—crystalline. In the NFS time-domain

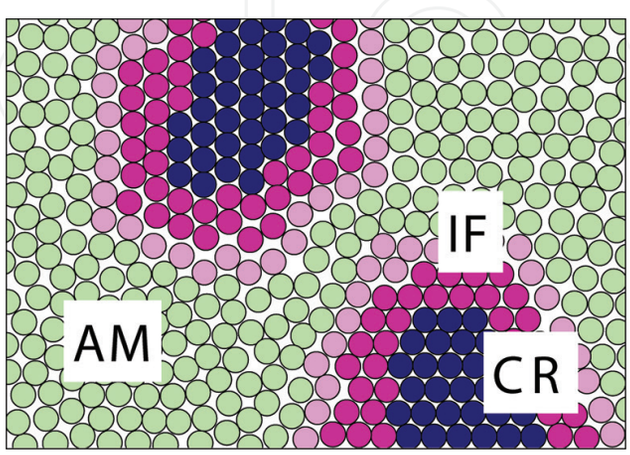

Figure 3. Schematic representation of a nanocrystalline structure that includes the residual amorphous matrix (light green)—AM, inner parts (core) of nanocrystalline grains (dark blue)—CR, and interfacial regions (violet)—IF.

patterns, it is refined by a sharp value of magnetic hyperfine field. The third structural component is interpreted as interface region (IF) between the former two structures. It constitutes a shell of the nanograins with undeveloped crystal symmetry. During the evaluation, it is refined by a distribution of hyperfine magnetic fields. Schematic representation of this concept is presented in **Figure 3**.

Hyperfine parameters of all fitting components evolve with temperature/time of the experiment. Eventually, at certain temperatures (e.g., Curie temperature, onset of crystallization), qualitatively different hyperfine interactions appear. Consequently, the physical model should reflect this situation by the use of appropriate type of distributions of hyperfine parameters (magnetic fields vs. quadrupole splitting). Proper type of distribution in certain temperature/time region is chosen by the help of the Hubert software [32].

5. Structural transformations in metallic glasses

5.1. Dynamical experiments

Effects of continuously changing temperature on magnetic ordering and structural transformation in MGs are demonstrated using the $(Fe_{2.85}Co_1)_{77}Mo_8Cu_1B_{14}$ amorphous alloy. This chemical composition ensures ferromagnetic states of the as-quenched MG at room temperature. Corresponding NFS time-domain patterns are plotted in **Figure 4**.

It should be stressed that the NFS time-domain patterns in **Figure 4** are in fact raw measured data as obtained directly from the experiment. Even without any quantitative evaluation, two qualitative changes in the character of interferograms are clearly observed at ~247 and ~435 °C. They are associated with magnetic and structural transformation, respectively, characterized

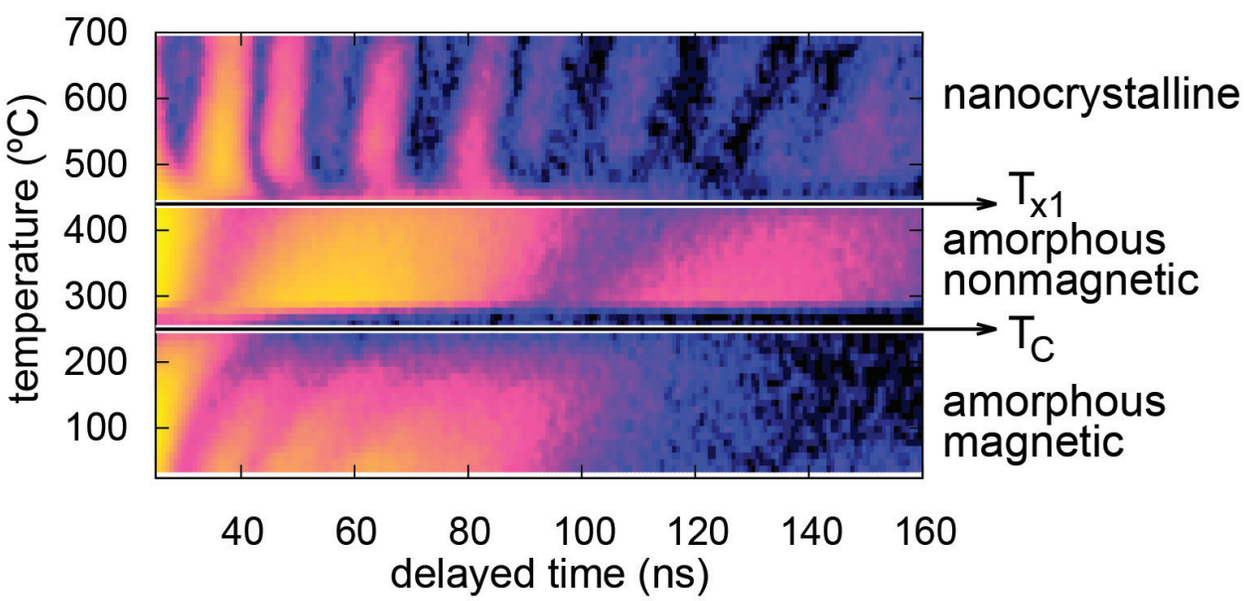

Figure 4. Contour plot of NFS time-domain patterns accumulated during dynamic annealing of the $(Fe_{2.85}Co_1)_{77}Mo_8Cu_1B_{14}$ MG. Heating rate is 10 K/min.

http://dx.doi.org/10.5772/66869

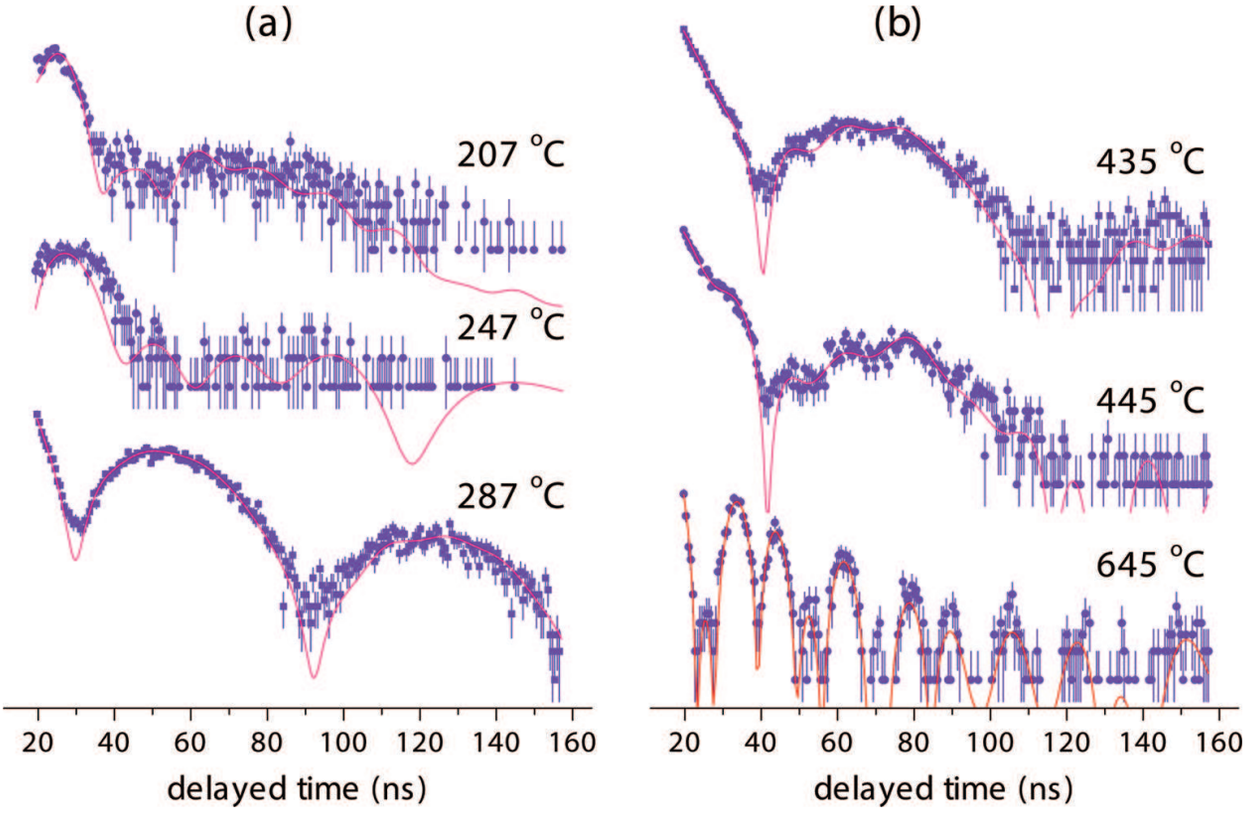

Figure 5. NFS time-domain patterns of the $(Fe_{2.85}Co_1)_{77}Mo_8Cu_1B_{14}$ MG taken at the vicinity of T_C (a) and T_{x1} (b) at the indicated temperatures.

by Curie T_C and crystallization T_{x1} temperatures. Consequently, the whole temperature region can be divided into three areas where the investigated MG exhibits magnetic amorphous, nonmagnetic amorphous, and magnetic nanocrystalline structure as it is shown in **Figure 4**.

In order to illustrate the alternations in the shapes of NFS time-domain patterns, selected individual records are plotted in **Figure 5**. It should be noted that the thickness effect of the sample has an important impact on the time-domain patterns. It results in the so-called hybrid beat character [34] which alternates their shapes.

With increasing temperature during the dynamic experiment, we can observe shift of the quantum beats maxima towards higher delayed times. Simultaneously, their intensities decrease. These effects are connected with vanishing hyperfine magnetic fields as a function of temperature. Magnetic quantum beats eventually fade away when the temperature reaches T_C and the Zeeman sextet collapses. At this temperature, the six de-excitation photons have comparable energies that are moreover overlapped within the line width. The resulting interference pattern in time domain exhibits very fast time decay, and the corresponding NFS time-domain pattern nearly disappears. This situation is demonstrated in **Figure 5a** where selected records taken at the vicinity of T_C~247 °C are plotted.

Formation of nanocrystalline bcc-(Fe,Co) grains during the first crystallization step resumes magnetic interactions that are identified by the corresponding quantum beats in **Figure 5b**.

For comparison, NFS time-domain patterns at 435, 445, and 645 °C were chosen. At 435 °C, the the sample is still fully amorphous and paramagnetic, that is, only electric quadrupole interactions are present (compare **Figure 1d**). With the onset of nanocrystallization, more rapid oscillations, which represent hyperfine magnetic fields, appear in time region 43–83 ns. At 445 °C, they are already satisfactorily visible. Finally, at 645 °C, the NFS time-domain pattern clearly shows well-developed magnetic structure (see also **Figure 1f**) which means that the degree of crystallization is significantly high.

The temperature of the onset of the first crystallization T_{x1} can be, however, accurately determined taking into consideration the whole temperature dependence of relative areas of amorphous (AM) and crystalline (CR) fitted components plotted in **Figure 6**. The total number of counts, that is, the overall area under time-domain patterns, is also provided. Here, the local minimum at ~247 °C indicates T_C of the amorphous matrix. The successive abrupt increase is associated with magnetic transformation inside the amorphous matrix. Further continuous decrease in the total counts is caused by temperature dependence of the f-factor. The onset of nanocrystallization is documented in **Figure 6a** by a notable change in the slope of the curve where the inflection point represents T_{x1} ~435 °C. The same T_{x1} is derived from temperature dependence of relative area of the CR component in **Figure 6b**. Surface crystallization starts at somewhat lower T_{x1} ~410 °C as confirmed by CEMS measurements [35].

The onset of crystallization changes the character of the beats. When new nanocrystalline grains appear, a magnetic order is established among the newly formed bcc-(Fe,Co) grains. This is indicated by an occurrence of dipole magnetic interactions that exhibit themselves by high-frequency oscillations in the corresponding NFS time-domain patterns in **Figures 4** and **5b**. The behaviour of the amorphous matrix with temperature is more complex. It can be followed by evolution of hyperfine magnetic fields in the temperature region where the system is ferromagnetic and by quadrupole splitting values at $T>T_C$. Both parameters are plotted in **Figure 7**.

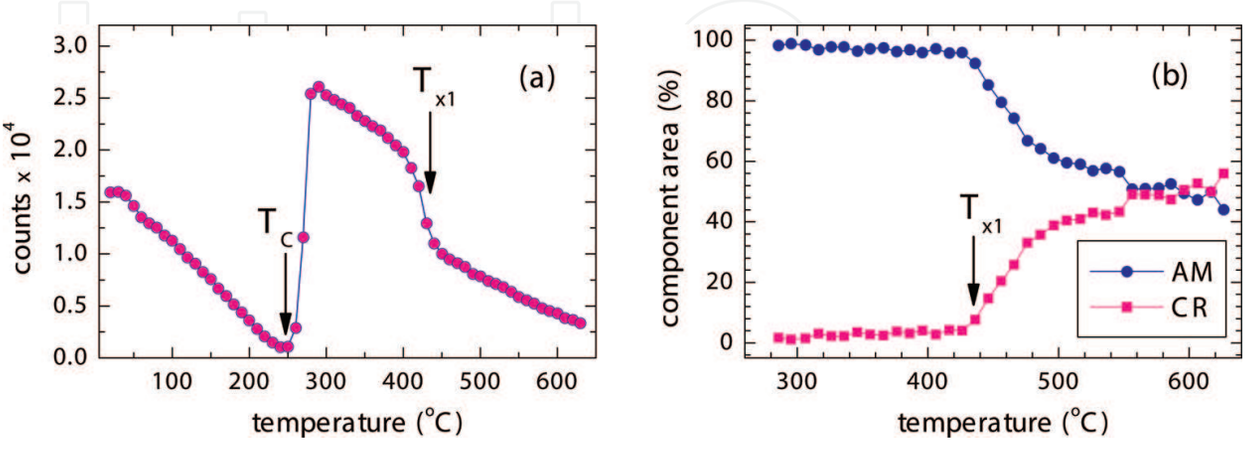

Figure 6. Total number of counts (spectral area) (a) and relative fractions of AM and CR components (b) of NFS time-domain patterns of the $(Fe_{2.85}Co_1)_{77}Mo_8Cu_1B_{14}$ MG plotted against temperature. Transition temperatures T_C and T_{x1} are marked with arrows.

http://dx.doi.org/10.5772/66869

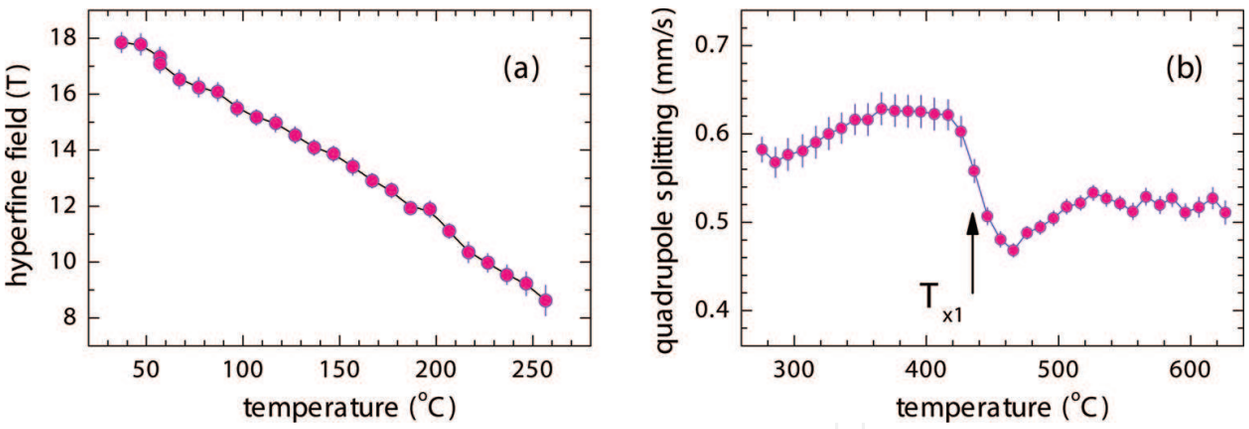

Figure 7. Average hyperfine magnetic field (a) and quadrupole splitting (b) values of the amorphous matrix in the $(Fe_{2.85}Co_1)_{77}Mo_8Cu_1B_{14}$ MG plotted against temperature.

For temperatures up to T_C, the hyperfine magnetic fields continuously decrease till they acquire values that are comparable in strength with electric quadrupole interactions. It should be noted that both types of hyperfine interactions coexist in some temperature range. In fact, it is impossible to distinguish between them also because of low total number of counts in the NFS time-domain patterns (see **Figures 5a** and **6a**). Here, the fitting is accomplished by two qualitatively distinct models, viz. distribution of hyperfine magnetic fields and distribution of quadrupole splitting. They are applied in certain temperature regions that approach T_C from bottom (i.e., $T<T_C$) and from top ($T_C<T$), respectively, with some small overlap [32].

Temperature evolution of quadrupole splitting provides information about bond properties and local symmetry of the iron sites in the AM phase. It shows a local minimum in **Figure 7b**. The associated inflection point indicates T_{x1}. Above this onset of nanocrystallization, the residual AM phase still persists, and when the CR phase is well developed (T>~500 °C), the average quadrupole splitting is stabilized.

To summarize the above discussion, we would like to note that the $(Fe_{2.85}Co_1)_{77}Mo_8Cu_1B_{14}$ MG was intentionally chosen to demonstrate the possibilities of dynamical NFS experiments. It is possible to follow on fly not only the evolution of its structural arrangement but also that of hyperfine magnetic interactions.

5.2. Dynamical experiments in external magnetic field

In order to improve magnetic parameters of nanocrystalline alloys, crystallization of metallic glasses often takes place under external magnetic field, the so-called magnetic annealing [36]. It results in appearance of induced magnetic anisotropy in heat-treated soft MGs. Nevertheless, all studies are performed ex situ after the magnetic annealing. Naturally, a question has arisen how external magnetic field affects the progress of nanocrystallization.

Similar as in the previous experiment, in situ investigations can be effectively performed by dynamical increase of temperature without and with external magnetic field by employing the NFS technique. But now, we have selected MG that is almost purely paramagnetic at

room temperature, namely $Fe_{81}Mo_8Cu_1B_{10}$. Only minute amounts of surface crystallization were unveiled by CEMS [37] on both sides of ribbon-shaped samples.

The reason for choosing this MG was twofold: (i) this chemical composition leads to formation of bcc-Fe nanocrystals, and iron is a calibration material for these studied; hence, its hyperfine parameters are well known, and (ii) the fitting model used for evaluation of the experimental NFS data is more simple because the residual amorphous matrix is paramagnetic, and only distributions of quadrupole splitting are used. On the other hand, formation of bcc-Fe nanograins imposes magnetic dipole interactions that are represented by single hyperfine magnetic field value. As described in the Section 4.2, iron atoms located in interface regions can be also identified via distribution of hyperfine magnetic fields. Consequently, temperature evolution of three structurally different regions in the investigated MG can be studied.

Contour plots of NFS time-domain patterns recorded during continuous increase of temperature in zero-field conditions and with applied external magnetic field (0.652 T) are shown in **Figure 8**. Dramatic impact of this rather small external magnetic field upon dynamics of the crystallization process is clearly seen. The plotted experimental data exhibit obvious modifications of hyperfine interactions that are reflected in the shapes of NFS time-domain patterns. At room temperature, the investigated $Fe_{81}Mo_8Cu_1B_{10}$ MG is amorphous, and in zero-field conditions, it demonstrates prevailing electric quadrupole interactions with hardly visible beatings of magnetic origin (due to surface crystallization). With the onset of nanocrystallization, contribution of magnetic dipole interactions becomes better visible in **Figure 8a** in the vicinity of ~400 °C. Appearance of hyperfine magnetic fields is remarkably accelerated when the annealing is performed in external magnetic field. In **Figure 8b**, the same character of NFS time-domain pattern is observed earlier at a temperature that is by about 100 °C lower.

Quantitative and qualitative description of the time-domain patterns is presented in **Figure 9** as derived from zero-field and in-field NFS experiments. Relative amounts of individual

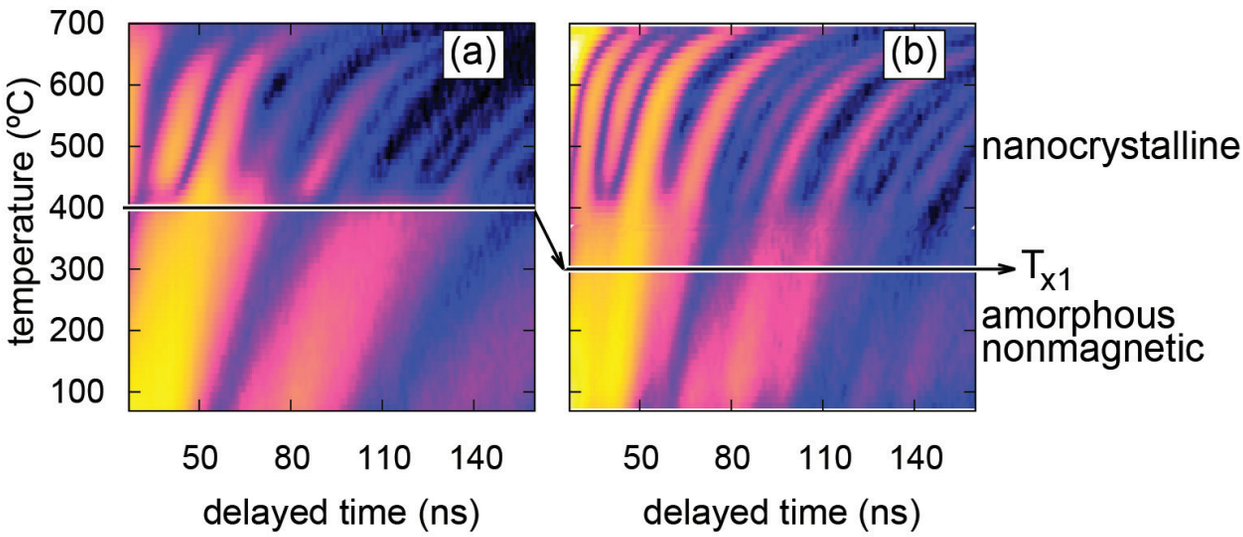

Figure 8. Contour plots of NFS time-domain patterns of the $Fe_{81}Mo_8Cu_1B_{10}$ MG measured without (a) and with external magnetic field of 0.652 T (b).

components comprising relative areas of the amorphous (AM) and total nanocrystalline (CR+IF) phases are shown in **Figure 9a**. It is noteworthy that the onset of crystallization should be determined from the temperature dependences of the relative areas rather than from the contour plots in **Figure 8**. In the latter, intensities of the NFS time-domain patterns are plotted in logarithmic scale, and thus, the applied colour-coded scale is coarse to a certain extent. Consequently, fine details of the particular line shapes might not be properly seen.

Presence of small number of quenched-in nanocrystallites (~10 %) that were formed during the production of the ribbons was unveiled by the help of **Figure 9a**, too. They were accounted for the fitting model by introducing a component with well-defined hyperfine magnetic fields. The obtained temperature dependences are shown in **Figure 9b**. Hyperfine fields corresponding to nanocrystalline grains are compared with those of a polycrystalline bcc-Fe foil. The former exhibit systematically lower values which are caused by small amounts as well as dimensions of quenched-in nanocrystals.

At certain temperature of annealing, additional nanocrystalline grains appear, and all grains begin to grow both in number and in size. This rather abrupt onset of bulk nanocrystallization is clearly seen by a step-like increase in the hyperfine magnetic field value at ~400 °C during annealing in zero-field conditions. Under the influence of external magnetic field, this increase is rather continuous but starts at ~300 °C, that is, much earlier. For T>400 °C, both curves merge together and follow the temperature dependence of hyperfine magnetic fields that correspond to bulk bcc-Fe with almost constant difference of ~2 T. Lower hyperfine magnetic field values are due to small dimensions of the nanocrystals.

It is noteworthy that the decrease of hyperfine magnetic field with temperature as observed in **Figure 9**b is also demonstrated in **Figure 8** by shift of the maxima of time-domain patterns towards higher delayed times. With rising temperature, the magnetic ordering continuously vanishes and eventually disappears at the Curie point.

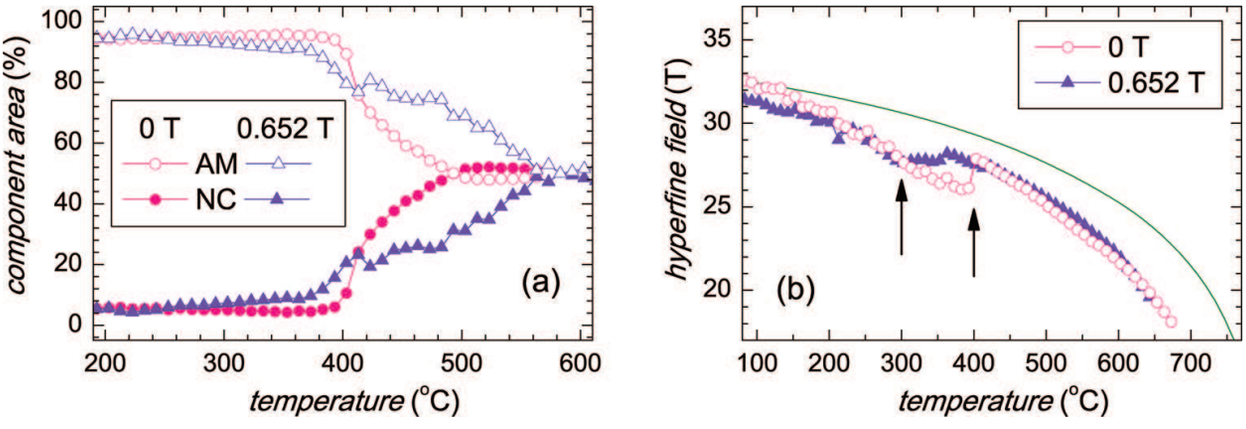

Figure 9. Relative amounts of amorphous (AM) (open symbols) and total nanocrystalline (NC=CR+IF) (solid symbols) components (a) and hyperfine magnetic fields of nanocrystals (b) plotted against temperature of annealing as obtained from NFS time-domain patterns of the $Fe_{81}Mo_8Cu_1B_{10}$. MG measured in zero magnetic field (circles) and in the field of 0.652 T (triangles). Values corresponding to bulk bcc-Fe (green curve) are given for comparison. The arrows indicate T_{x1}.

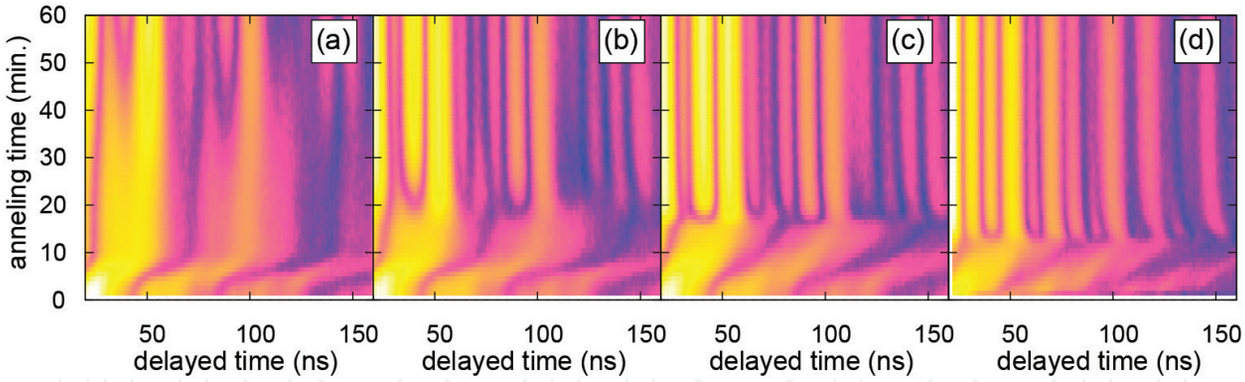

Figure 10. Contour plots of isothermal NFS time-domain patterns of the $Fe_{90}Zr_7B_3$ MG annealed at 470 °C (a), 480 °C (b), 510 °C (c), and at 480 °C under external magnetic field of 0.652 T (d).

In this section, we have demonstrated how NFS experiments can contribute to more detail description of structural as well as magnetic transformations that are taking place in real time upon MGs exposed to dynamically changing temperature. In particular, in situ studies of hyperfine interactions cannot be performed by any other analytical tool. Thus, a possibility to follow separately temperature evolution of individual structural components viz. AM, CR, and IF makes NFS an interesting and competitive method for the investigation of nanocrystallization in MGs *during* its progress. In the following section, other aspects of this technique are presented with a special focus at time-dependent experiments.

5.3. Isothermal experiments

In the above section, we have concentrated on a dynamics of nanocrystallization. For that purpose, a continuous increase of temperature with a constant ramp was ensured. Acquisition of NFS data was accomplished in situ during ongoing progress of temperature. Thus, the investigated system was exposed to change annealing conditions. Here, we focus at the kinetics of crystallization. The studies were performed at constant annealing conditions. In this way, information on various parameters of the crystallization kinetics can be acquired.

NFS experiments were performed on $Fe_{90}Zr_7B_3$ MG prepared by melt spinning technique in a form of thin ribbons. After initial rapid increase of temperature with a ramp of 40 K/min, the annealing temperature was stabilized at its destination value. NFS data were recorded *in situ* with an acquisition time of 1 min. Duration of the experiments was up to 150 min. The annealing temperatures of 470, 480, and 510 °C were chosen. Isothermal experiment at 480 °C was performed also in an external magnetic field of 0.652 T.

Contour plots of NFS time-domain patterns from all experiments are shown in **Figure 10**. Time of annealing under the set conditions is given on the y-axes. The originally as-quenched sample is paramagnetic at room temperature and exhibits quantum beats typical for electric quadrupole interactions (see **Figure 1d**). Depending upon the annealing conditions, newly formed ferromagnetic nanocrystalline grains of bcc-Fe emerge from the amorphous matrix within 10–30 min after reaching the annealing temperature. They are identified through magnetic dipole interactions that give rise to hyperfine magnetic fields. The latter exhibit well-developed high-frequency oscillations in quantum beats similar as those in **Figure 1f**. They

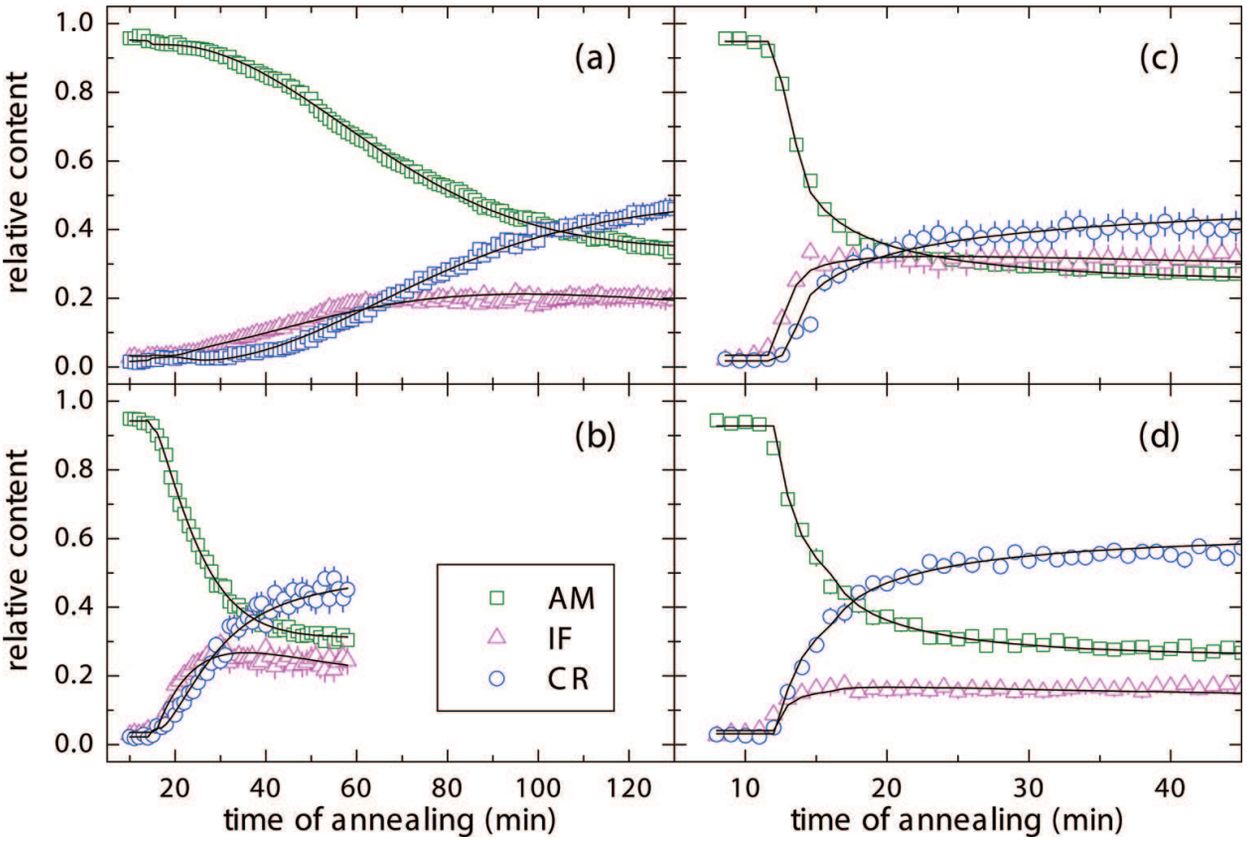

Figure 11. Relative amounts of structural components including amorphous matrix (AM, green squares), crystalline grains (CR, blue circles), and interface regions (IF, magenta triangles) plotted against time of annealing at 470 °C (a), 480 °C (b), 510 °C (c), and at 480 °C under external magnetic field of 0.652 T (d). Solid curves represent fits according to the crystallization model introduced in Ref. [18].

persist over the entire time of the experiments. Because the temperature of annealing does not change, the positions of individual beat maxima are also stable.

Time evolution of individual structural components viz. AM, CR, and IF is presented in **Figure 11**. Relative areas obtained from evaluation of NFS time-domain patterns are displayed by symbols. Subsequently, they were fitted using a crystallization model introduced recently [18]. The resulting theoretical curves are plotted by solid lines. The following observations can be noted. First, as demonstrated by the IF and CR relative contents in **Figure 11a** and **b**, the IF component dominates that of the CR one during the first 65 and 30 min of annealing, respectively. This indicates that the grains are rather small and thus exhibit higher contribution of the atoms located at their surfaces. Later, the grains grow in size which is documented by a higher fraction of CR than IF. The latter saturate with time which means that the grains do not grow any further, and only their number increases.

Secondly, increase in temperature of annealing from 470 to 480 °C accelerates formation of nanograins. In order to achieve ~60 % of nanograins, three times shorter time is needed for annealing temperature of 480 °C in comparison with 470 °C. Note different scales on the x-axes. Further temperature increase from 480 to 510 °C expectedly speeded-up the crystallization rate as seen in **Figure 11c**. The same effect is reached, however, by annealing at the

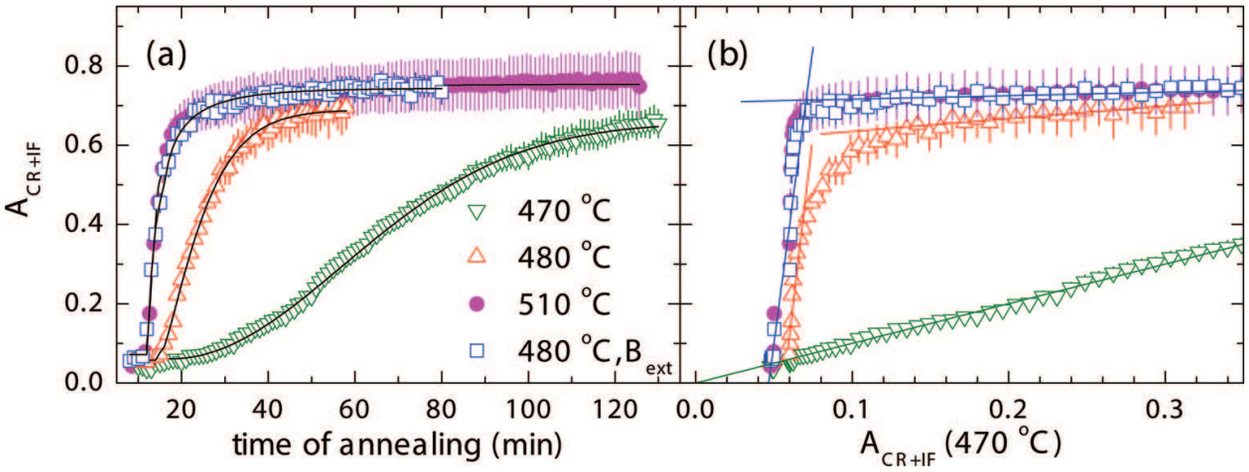

Figure 12. Relative amount of nanograins A_{CR+IF} plotted against time of annealing (a) and relative content of nanograins obtained at 470 °C (b). Black solid curves in (a) represent fit according to the crystallization model introduced in Ref. [18].

lower temperature of 480 °C in external magnetic field of 0.652 T as demonstrated in **Figure 11d**. The time needed for crystallization is by a factor of ~3 less than that without the external magnetic field at the same temperature of annealing.

Relative content of nanocrystals given as a sum of the corresponding crystalline (CR) and interface (IF) components A_{CR+IF} is depicted in **Figure 12**. Formation of nanograins under different annealing conditions is mutually compared in **Figure 12a** with respect to the annealing time. As discussed above, small increase in the annealing temperature from 470 to 480 °C, that is, only by 10 °C causes notable increase in the amount of nanograins that are formed during the same time period. This is due to proximity of the first crystallization temperature. When the annealing temperature is elevated further to 510 °C (i.e., by 30 °C), the change in the character of the A_{CR+IF} dependence is not so dramatic. We stress again, that almost the same contents of nanograins is obtained when annealing at 480 °C proceeds under weak magnetic field. Presumably, this is caused by huge influence of small energetic perturbations of magnetic interactions in comparison with the thermal energy.

Figure 12a shows absolute values of the nanocrystalline content, and as it is more closely discussed elsewhere [19], all processes behave identically from a qualitative point of view. Dramatic differences among them are revealed, however, by the help of **Figure 12b**. Here, the total amount of nanograins A_{CR+IF} is plotted against this parameter obtained from the slowest isothermal experiment performed at 470 °C. Consequently, the experimentally acquired data are distributed along a straight line with the slope equal 1. Dramatic changes in the slopes are observed during annealing at 480, 510, and 480 °C in external magnetic field. The associated rates of nanocrystallization are by a factor of ~30 higher that at 470 °C. They are indicated in **Figure 12b** by straight almost vertical lines. In order to visualize these rapid processes more clearly, the x-axis is reduced to the equivalent of the first ~65 min of the isothermal experiments.

After the initial rapid onset of nanocrystals formation, further increase in A_{CR+IF} is not so steep. In fact, it almost saturates with the slope of 0.1 for annealing at 510 °C and at 480 °C

http://dx.doi.org/10.5772/66869

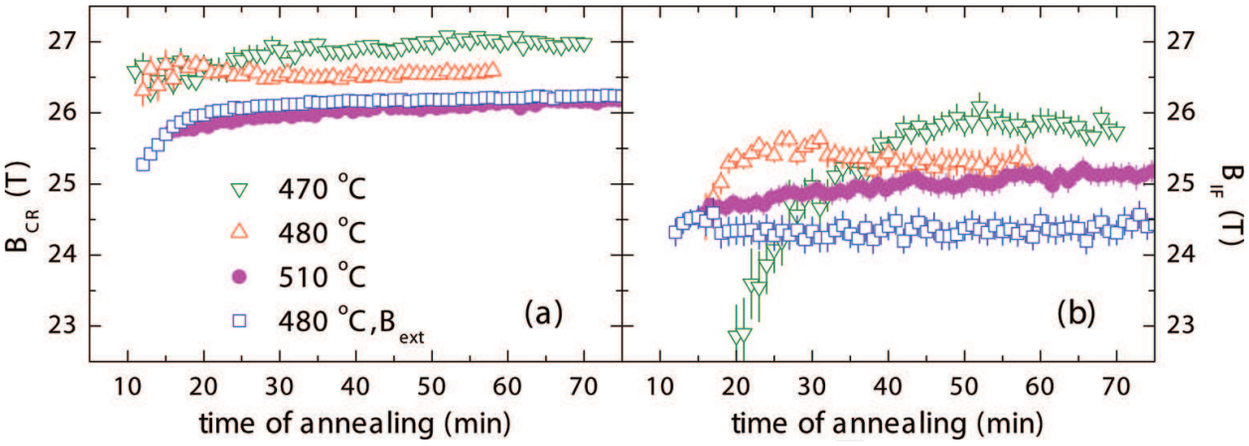

Figure 13. Hyperfine magnetic field of the CR (a) and IF (b) components plotted against time of annealing.

in B_{ext} = 0.652 T. In zero-field annealing at 480 °C, it exhibits only gentle increase towards the same saturation value showing slightly higher slope of 0.32.

Hyperfine magnetic fields obtained from the CR and IF components are depicted in **Figure 13** as a function of annealing time. Depending upon the temperature of annealing, B_{CR} saturates at different values as seen in **Figure 13a**. They are by about 1.5 T smaller than those of polycrystalline bcc-Fe [38] due to nanosized dimensions of the grains. Decrease in B_{CR} at the beginning of annealing especially at 480 °C in B_{ext} indicates that the inner structure of bcc nanograins is still not very well developed during early stages of crystallization. Similar phenomenon is observed in **Figure 13b** where hyperfine magnetic fields of the interface components B_{IF} are presented.

Small dimensions of nanocrystalline grains are also responsible for remarkable time evolution of B_{IF} especially during annealing at 470 °C and to a smaller extent at 480 °C. At the beginning of grain growth, majority of the constituent Fe atoms is located at the surfaces of the nanocrystals. As a result, relative content of the IF component prevails that of the CR one as demonstrated in **Figure 11a** and **b.** Simultaneously, because of symmetry breaking in the interfacial regions, the associated hyperfine magnetic fields exhibit smaller values than the inner parts of the grains.

In this section, we have demonstrated how NFS can be used for the investigations of the kinetics of crystallization. Isothermal experiments performed under different annealing conditions, viz. temperature and presence of external magnetic field provide valuable information on the time evolution of both the content of nanocrystals and on their hyperfine magnetic fields. Moreover, these phenomena can be studied separately for structurally different regions that are found in NCAs.

6. Conclusions

Nanocrystallization of metallic glasses was followed by in situ experiments of nuclear forward scattering (NFS) of synchrotron radiation to fine details that are completely hidden when conventional analytical tools are employed. Detailed analyses of NFS time-domain patterns that were decomposed into contributions stemming from the amorphous residual phase and newly

formed nanocrystallites provided an opportunity to study independently the role of structurally different regions. Moreover, using this approach, it was possible to further differentiate between contributions from the surfaces and the inner parts of nanograins. Different amounts of iron atoms located at the grains' surfaces and in their bulk were observed when different crystallization conditions, viz. temperature and/or external magnetic field, were applied.

The application of in situ NFS experiments has a huge potential for observations of the evolution of phase transformations in real time performed on fly during short time intervals. This was documented by two types of in situ NFS experiments. Namely, dynamical temperature increase and isothermal annealing under constant conditions were applied. It was possible to follow not only structural transformations, but, at the same time, also changes in magnetic arrangement were revealed. The latter is feasible owing to rapid screening of the corresponding hyperfine interactions. In this way, detail information about the nearest neighbourhoods of the resonant atoms is experimentally achievable. Moreover, the local arrangements can be checked in real time thus enabling structural and/or magnetic transformation to be followed on fly. In addition, a possibility of comparing the experimental results with those obtained from simulations and/or theoretical calculations is offered. Such experiments are unique and open new horizons in materials research by employing the technique of nuclear forward scattering of synchrotron radiation.

Acknowledgements

We are grateful to R. Rüffer (Grenoble) and S. Stankov (Karlsruhe) for stimulating discussions. Samples of metallic glasses were provided by a courtesy of D. Janičkovič (Bratislava). The authors would like to thank P. Švec (Bratislava), J. Kohout (Prague), and A. Lančok (Husinec-Řež) for their technical assistance during measurements on the synchrotron and V. Vrba (Olomouc) for his help with data processing. Financial support of the grants GAČR 14-12449S, IGA_PrF_2016_022, and VEGA 1/0182/16 is acknowledged.

Author details

Marcel B. Miglierini[1,2]* and Vít Procházka[3]

*Address all correspondence to: marcel.miglierini@stuba.sk

1 Slovak University of Technology in Bratislava, Faculty of Electrical Engineering and Information Technology, Institute of Nuclear and Physical Engineering, Bratislava, Slovakia

2 Department of Nuclear Reactors, Faculty of Nuclear Science and Physical Engineering, Czech Technical University in Prague, Prague, Czech Republic

3 Department of Experimental Physics, Faculty of Science, Palacky University, Olomouc, Czech Republic

References

[1] Herzer G. Modern soft magnets: Amorphous and nanocrystalline materials. Acta Mater. 2013;**61**,718–734. doi:10.1016/j.actamat.2012.10.040

[2] McHenry ME, Willard MA, Laughlin DE. Amorphous and nanocrystalline materials for applications as soft magnets. Prog Mater Sci. 1999;**44**,291–443. doi:10.1016/S0079-6425(99)00002-X

[3] McHenry ME, Laughlin DE. Nano-scale materials development for future magnetic applications. Acta Mater. 2000;**48**,223–238. doi:10.1016/S1359-6454(99)00296-7

[4] Gutfleisch O, Willard MA, Bruck E, Chen CH, Sankar S, Liu JP. Magnetic materials and devices for the 21st century: stronger, lighter, and more energy efficient. Adv Mater. 2011;**23**,821–842. doi:10.1002/adma.201002180

[5] Hernando A. Magnetic properties and spin disorder in nanocrystalline materials. J Phys: Condens Matter. 1999;**11**,9455–9482. doi:10.1088/0953-8984/11/48/308

[6] Inoue A, Takeuchi A. Recent development and application products of bulk glassy alloys. Acta Mater. 2011;**59**,2243–2267. doi:10.1016/j.actamat.2010.11.027

[7] Miglierini M, Kopcewicz M, Idzikowski B, Horváth ZE, Grabias A, Škorvánek I, Dluzewski P, Daróczi CsC. Structure, hyperfine interactions and magnetic behavior of amorphous and nanocrystalline $Fe_{80}M_7B_{12}Cu_1$ (M = Mo, Nb, Ti) alloys. J Appl Phys. 1999;**85**,1014–1025. doi:10.1063/1.369223

[8] Pavuk M, Miglierini M, Vujtek M, Mashlan M, Zboril R, Jiraskova Y. AFM and Mössbauer spectrometry investigation of the nanocrystallization process in Fe-Mo-Cu-B rapidly quenched alloy. J Phys: Condens Matter. 2007;**19**,216219. doi:10.1088/0953-8984/19/21/216219

[9] Miglierini M., Lančok A, Kohout J. Hyperfine fields in nanocrystalline Fe-Zr-B probed by 57Fe nuclear magnetic resonance spectroscopy. J Appl Phys Lett. 2010;**96**,211902. doi:10.1063/1.3431612

[10] Pradeep KG, Herzer G, Choi P, Raabe D. Atom probe tomography study of ultrahigh nanocrystallization rates in FeSiNbBCu soft magnetic amorphous alloys on rapid annealing. Acta Mater. 2014;**68**,295–309. doi:10.1016/j.actamat.2014.01.031

[11] Mattern N, Stoica M, Vaughan G, Eckert J. Thermal behaviour of $Pd_{40}Cu_{30}Ni_{10}P_{20}$ bulk metallic glass. Acta Mater. 2012;**60**,517–534. doi:10.1016/j.actamat.2011.10.032

[12] Wang G, Mattern N, Bednarčík J, Li R, Zhang B, Eckert J. Correlation between elastic structural behavior and yield strength of metallic glasses. Acta Mater. 2012;**60**,3074–3084. doi:10.1016/j.actamat.2012.02.012

[13] Egami T, Tong Y, Dmowski W. Deformation in metallic glasses studied by synchrotron X-ray diffraction. Metals. 2016;**6**,22.doi:10.3390/met6010022

[14] Puncreobutr C, Phillion AB, Fife JL, Rockett P, Horsfield AP, Lee PD. In situ quantification of the nucleation and growth of Fe-rich intermetallics during Al alloy solidification. Acta Mater. 2014;**79**,292–303. doi:10.1016/j.actamat.2014.07.018

[15] Giordano VM, Ruta B. Unveiling the structural arrangements responsible for the atomic dynamics in metallic glasses during physical aging. Nat Commun. 2016;**7**,10344. doi:10.1038/ncomms10344

[16] Miglierini M, Greneche J-M. Mössbauer spectrometry of Fe(Cu)MB-type nanocrystalline alloys: II. The topography of hyperfine interactions in Fe(Cu)ZrB alloys. J Phys: Condens Matter. 1997;**9**,2321–2347. doi:10.1088/0953-8984/9/10/018

[17] Smirnov GV. General properties of nuclear resonant scattering. Hyperfine Int. 1999;**123/124**,31–77. doi:10.1023/A:1017007520099

[18] Miglierini M, Prochazka V, Stankov S, Svec Sr. P, Zajac M, Kohout J, Lancok A, Janickovic D, Svec P. Crystallization kinetics of nanocrystalline alloys revealed by in-situ nuclear forward scattering of synchrotron radiation. Phys Rev B. 2012;**86**,020202(R). doi:10.1103/PhysRevB.86.020202

[19] Miglierini M, Procházka V, Rüffer R, Zbořil R. In situ crystallization of metallic glasses during magnetic annealing. Acta Mater. 2015;**91**,50–56. doi:10.1016/j.actamat.2015.03.012

[20] Procházka V, Vrba V, Smrčka D, Rüffer R, Matúš P, Mašláň M, Miglierini M. Structural transformation of NANOPERM-type metallic glasses followed in situ by synchrotron radiation during thermal annealing in external magnetic field. J Alloy Compds. 2015;**638**,398–404. doi:10.1016/j.jallcom.2015.03.058

[21] Miglierini M, Pavlovič M, Procházka V, Hatala T, Schumacher G, Rüffer R. Evolution of structure and local magnetic fields during crystallization of HITPERM glassy alloys studied by in situ diffraction and nuclear forward scattering of synchrotron radiation. Phys Chem Chem Phys. 2015;**17**,28239–28249. doi:10.1039/C5CP00245A

[22] Machala L, Procházka V, Miglierini M, Sharma VK, Marušák Z, Wille HCh, Zbořil R. Direct evidence of Fe(V) and Fe(IV) intermediates during reduction of Fe(VI) to Fe(III): a nuclear forward scattering of synchrotron radiation approach. Phys Chem Chem Phys. 2015;**17**,21787–21790. doi:10.1039/c5cp03784k

[23] Stankov S, Yue YZ, Miglierini M, Sepiol B, Sergueev I, Chumakov AI, Hu L, Švec P, Rüffer R. Vibrational properties of nanograins and interfaces in nanocrystalline materials. Phys Rev Lett. 2008;**100**,235503. doi:10.1103/PhysRevLett.100.235503

[24] Stankov S, Miglierini M, Chumakov AI, Sergueev I, Yue YZ, Sepiol B, Svec P, Hu L, Rüffer R. Vibrational thermodynamics of NANOPERM nanocrystalline alloy from nuclear inelastic scattering. Phys Rev B. 2010;**82**,144301. doi:10.1103/PhysRevB.82.144301

[25] Röhlsberger R. Nuclear Condensed Matter Physics with Synchrotron Radiation. Berlin Heidelberg: Springer-Verlag; 2004. 318 p. doi:10.1007/b86125

[26] Seto M. Condensed matter physics using nuclear resonant scattering. J Phys Soc Jpn. 2013;**82**,021016. doi:10.7566/JPSJ.82.021016

[27] Gütlich Ph, Bill E, Trautwein AX. Mössbauer Spectroscopy and Transition Metal Chemistry. Heilderberg Dordrecht London New York: Springer; 2011. 568 p. doi:10.1007/978-3-540-88428-6

[28] Rüffer R. Nuclear resonance scattering. CR Physique. 2008;**9**,595–607. doi:10.1016/j.crhy.2007.06.003

[29] Sturhahn W, Gerdau E. Evaluation of time-differential measurements of nuclear-resonance scattering of x rays. Phys Rev B. 1994;**49**,9285–9294. doi:10.1103/PhysRevB.49.9285

[30] Sturhahn W. CONUSS and PHOENIX: Evaluation of nuclear resonant scattering data. Hyperfine Interact. 2000;**125**,149–172. doi:10.1023/A:1012681503686

[31] Hubert software package [Internet]. 2015. Available from: http://fyzika.upol.cz/cs/vysledky-vyzkumu/software-hubert [Accessed: 2016-08-18].

[32] Vrba V, Procházka V, Smrčka D, Miglierini M. Hubert: Software for efficient analysis of in-situ nuclear forward scattering experiments. In: AIP Conference Proceedings **1781**, 020013 (2016); doi:10.1063/1.4966009

[33] Miglierini M, Greneche J-M. Mössbauer spectrometry of Fe(Cu)MB-type nanocrystalline alloys: I. The fitting model for the Mössbauer spectra. J Phys: Condens Matter. 1997;**9**,2303–2319. doi:10.1088/0953-8984/9/10/017

[34] Shvyd'ko YV, van Burck U. Hybrid forms of beat phenomena in nuclear forward scattering of synchrotron radiation. Hyperfine Int. 1999;**123**,511–527. doi:10.1023/A:1017084209621

[35] Miglierini M, Hatala T, Frydrych J, Šafářová K. Surface crystallization of Co-containing NANOPERM-type alloys. Hyperfine Int. 2012;**205**,125–128. doi:10.1007/s10751-011-0495-1

[36] Škorvánek I, Marcin J, Turcanová J, Kovác J, Švec P. Improvement of soft magnetic properties in $Fe_{38}Co_{38}Mo_8B_{15}Cu$ amorphous and nanocrystalline alloys by heat treatment in external magnetic field. J Alloys Compd. 2010;**504**,S135–S138. doi:10.1016/j.jallcom.2010.04.033

[37] Miglierini M, Hatala T, Bujdoš M. Depth-selective study of surface crystallization in NANOPERM-type alloys. Acta Phys Pol A. 2014;**126**,56–57. doi:10.12693/APhysPolA.126.56

[38] Preston RS, Hanna SS, Heberle J. Mössbauer effect in metallic iron. Phys Rev B. 1962;**128**,2207–2218. doi:10.1103/PhysRev.128.2207

IntechOpen